# ORIGINAL PAPER



# On the fracture toughness of shape memory alloys

Mohammed Y. Alsawalhi · Chad M. Landis

Received: 27 March 2022 / Accepted: 17 May 2022 / Published online: 8 June 2022 © The Author(s), under exclusive licence to Springer Nature B.V. 2022

**Abstract** A phenomenological constitutive model for the thermomechanical constitutive behavior of shape memory alloys is implemented within finite element calculations to model the toughening due to the austenite to martensite phase transformation and martensite deformation during steady mode I crack growth. The process of heat generation during phase transformation near crack tip effects the temperature variations and thus the mechanical behavior of the material near the growing crack tip. Several dimensionless parameters relating the thermomechanical parameters of the constitutive model, the crack growth velocity, and the prevailing sample temperature are identified and applied to study the thermomechanical crack tip fields and the fracture toughness enhancement due to the nonlinear thermomechanical processes in the vicinity of the crack tip.

**Keywords** Shape memory alloys · Fracture toughness · Fracture mechanics

### 1 Introduction

Shape memory alloys (SMAs) have unique thermomechanical properties that allow them to experience large

M.Y. Alsawalhi · C.M. Landis (☒)
Department of Aerospace Engineering and Engineering
Mechanics, The University of Texas at Austin, Austin, TX,
USA

e-mail: landis@utexas.edu

type of pseudoelastic behavior occurs when the material is at a temperature where the austenite phase is stable and mechanical loading is applied which transforms the material into its martensite phase. A reversal of loading then allows for the reverse transformation from martensite to austenite. Additionally, while in the loaded martensite phase, a redirection of the applied stress state, e.g. from tension to shear, can also cause a macroscopic reorientation of the transformation strain of the martensite. Both of these behaviors is accompanied by a hysteresis in the stress versus strain behavior, which represents the dissipation of mechanical energy. With respect to the fracture properties of the material, this energy dissipation will result in an enhancement of the fracture toughness during crack growth. Moreover, the details of this toughening behavior are expected to be dependent on the velocity that the crack propagates. Slowly growing cracks will sample the isothermal behavior of the material because the latent heat that the material expels/absorbs can be readily conducted away from the crack tip. Conversely, fast growing cracks will sample the isentropic material behavior near the crack tip due to the lack of time available to conduct heat away. As such, the reduction in entropy associated with the transformation from austenite to martensite must be balanced by an increase in local temperature near the crack tip to provide a balancing increase in entropy. This may be thought of as an expul-

strains upon loading and then, depending on the tem-

perature, recover these strains upon unloading. This



sion of the latent heat of transformation, which in turn heats the material and tends to keep it in its austenite phase. The details of these behaviors are the topic of this study.

Nonlinear fracture mechanics concepts must be applied to SMAs due to the development of a phase transformation zone near the crack tip which has features that are both temperature and rate dependent (Maletta and Furgiuele 2010; Maletta et al. 2016). Consider a material point that experiences the passing of a nearby crack during the fracture of a pseudoelastic SMA at a nominal high temperature. Such a point traverses several features of SMA constitutive behavior. When the crack is far from this point, the response is linear elastic. As the point enters the elevated stress region near the crack tip it begins to transform from austenite to martensite. If the point is close enough to the tip then it may become fully transformed to martensite. As the point passes by the crack tip the reorientation of the martensite strain will occur due to the reorientation of the principal stress directions around the crack. Finally, once the point is sufficiently far from the tip, unloading occurs and the material returns to its original austenite state. Other material points that are not sufficiently close to the crack tip may not experience each of these regimes and may only undergo partial transformation, reorientation, and then recovery. In addition to the transformation strain and its evolution as the crack tip passes, latent heat is also expelled and absorbed during this process, and the resulting temperature change around the crack tip depends very sensitively on the relative speed at which the material can conduct heat away from the tip. The effects of such behavior on the fracture properties of SMAs requires a fully coupled thermomechanical field analysis, along with an assumption for the crack tip propagation criteria.

This work builds upon a variety of analytical and numerical work that studied the fracture of SMAs. Birman (1998) and Maletta and Furgiuele (2010) analyzed the extent of the austenite-to-martensite transformation zone around a stationary crack tip using a method analogous to the Irwin correction, Irwin (1960), for the plastic zone size. Maletta and Furgiuele (2010) confirmed their results for the extent of the transformation zone on the plane ahead of the crack tip using finite element calculations. Yi and Gao (2000) performed a transformation toughening-type of analysis, McMeeking and Evans (1982), to model the effects of martensitic transformation on the fracture tough-

ness under mixed-mode loading conditions. In line with prior phase-transformation toughening studies, they found that martensitic transformation reduces the crack tip energy release rate during steady crack growth and thus should increase the fracture toughness. Ardakani et al. (2015) performed numerical calculations that were very much in the same spirit as this paper, using the extended finite element method to analyze how the phase transformation causes temperature variations and alters the mechanical behavior in the vicinity of the crack tip. Their results showed a strong dependence of the crack growth behavior on the loading rate. The theoretical studies most similar to that presented here are due to Baxevanis et al. (2014a, b) who also applied multi-axial SMA constitutive models within steadystate finite element crack growth calculations to determine the contributions to toughening due to the dissipative effects of phase transformation. In this work non-isothermal rate dependent behaviors are considered while the prior works investigated the isothermal and isentropic limits.

In addition to these theoretical studies, there are several experimental studies that investigate features of the fracture of SMAs and the thermomechanical fields near crack tips. You et al. (2019) studied the temperature changes near a stationary crack tip in NiTi under cyclic loading and found that the experimental results were consistent with finite element calculations that implemented the constitutive model of Zaki and Moumni (2007). Specifically, they found that high frequency loading cycles increases the maximum temperature around the crack and decreases the size of the phase transformation region around the crack tip. This result was confirmed by their numerical simulations and is also consistent with the findings reported in this paper. Maletta et al. (2016) analyzed the stress-strain behavior near crack tip under thermomechanical loading conditions by using Digital Image Correlation to measure the displacement and strain responses near a stationary crack tip. They also measured a very interesting behavior that appears to be at odds with theoretical studies. They found that the fracture toughness of the low temperature martensite phase is smaller than that of the high temperature austenite phase and that the toughness of the austenite phase increases with increasing temperature. Given that this experimental result is seemingly contrary to theoretical studies, special attention is dedicated to its possible interpretation in the final discussion.



The purpose of this work is to study the effects of several important material, thermal, and crack growth parameters on the toughening behavior during steadystate crack growth in SMAs. The multi-axial phenomenological constitutive model is described and its fundamental stress-strain behaviors are illustrated. The model is applied within numerical simulations where the fields surrounding the crack-tip are analyzed using a specialized steady-state finite element method for crack growth in materials with irreversible constitutive behavior. Several sets of material parameters, prevailing temperatures, an crack growth velocities are considered, and their effects on the toughening behavior are presented. Finally, a discussion of the results of the present model and their relationship to existing experimental measurements is presented.

## 2 Material modeling

The non-isothermal thermomechanical SMA response is based on the constitutive model proposed by Alsawalhi and Landis (2021). This model is formulated using a single transformation surface defined in stress and temperature space. Additionally, it is a kinematic hardening model that utilizes an energetic "transformation potential" that allows the model to capture the forward transformation, the reverse transformation, and the reorientation of martensite phase during non-proportional stress loadings. This transformation potential is described in terms of internal variables using the invariants of the transformation strain and a transformation entropy variable that is akin to the martensite volume fraction and is closely related to the latent heat of transformation from martensite to austenite. Nearly all of the interesting features of SMA behavior are captured by the suitable formulation of the transformation potential, and details can be found in Alsawalhi and Landis (2021). Some notable features of the model include its ability to capturing the tension and compression asymmetry in strain, transformation stress in the pseudoelastic phase from austenite to martensite, and in the hardening.

Pertinent details of the constitutive model are outlined here. The transformation strain tensor,  $\varepsilon_{ij}^t$ , and transformation entropy,  $s^t$ , are employed as internal variables in this theory. The Helmholtz free energy of the material is postulated to take the form,

$$\Psi = \frac{1}{2} c_{ijkl} \left( \varepsilon_{ij} - \varepsilon_{ij}^t \right) \left( \varepsilon_{kl} - \varepsilon_{kl}^t \right) - \beta_{ij} \left( \varepsilon_{ij} - \varepsilon_{ij}^t \right) \theta$$

$$+ C \left( \theta - \theta_0 - \theta \ln \frac{\theta}{\theta_0} \right) - \theta s^t$$

$$+ \Psi^t (\varepsilon_{ij}^t, s^t) \tag{1}$$

The stress–strain–temperature–entropy relations are derived from this free energy as,

$$\sigma_{ij} = \frac{\partial \Psi}{\partial \varepsilon_{ij}} = c_{ijkl} \left( \varepsilon_{kl} - \varepsilon_{kl}^t \right) - \beta_{ij} \theta \tag{2}$$

$$s = -\frac{\partial \Psi}{\partial \theta} = \beta_{ij} \left( \varepsilon_{ij} - \varepsilon_{ij}^t \right) + C \ln \frac{\theta}{\theta_0} + s^t$$
 (3)

where  $c_{ijkl}$  denotes the elastic stiffness tensor,  $\sigma_{ij}$  is the stress tensor,  $\varepsilon_{ij}$  is the total strain tensor,  $\theta$  is the temperature, s is the total entropy,  $\beta_{ij}$  are the thermal stress moduli (which are related to the thermal expansion coefficients), and C is the heat capacity. The last term of Eq.(1) includes the transformation hardening potential  $\Psi^t$ , which depends only on the internal variables  $\varepsilon_{ij}^t$  and  $s^t$ . The first law of thermodynamics then is written as.

$$\underbrace{\dot{\Psi} + \theta \dot{s} + s \dot{\theta}}_{i} = \sigma_{ij} \dot{\varepsilon}_{ij} + r - q_{i,i} \tag{4}$$

Here, u is the internal energy per unit volume and  $q_i$  is the heat flux vector, and r is the external heat source per unit volume. The second law of thermodynamics can then be written in its point-wise form as,

$$\left(\sigma_{ij} - \sigma_{ij}^{B}\right) \dot{\varepsilon}_{ij}^{t} + \left(\theta - \theta^{B}\right) \dot{s}^{t} - \frac{1}{\theta} q_{i} \theta_{,i} \ge 0 \tag{5}$$

Here the "back stress" and "back temperature" are derived from the transformation potential as,

$$\sigma_{ij}^{B} = \frac{\partial \Psi^{t}}{\partial \varepsilon_{ij}^{t}} \tag{6}$$

$$\theta^B = \frac{\partial \Psi^t}{\partial s^t} \tag{7}$$

Eq. (5) is satisfied by adopting Fourier's law for the heat flux,  $q_i = -k_{ij}\theta_{,j}$ , and then by introducing a transformation surface in the space formed by  $\left(\sigma_{ij} - \sigma^B_{ij}\right)$  and  $\left(\theta - \theta^B\right)$ . For this work the following simple form for the transformation surface is chosen,



$$\Phi = \frac{3}{2} \frac{\left(s_{ij} - s_{ij}^{B}\right) \left(s_{ij} - s_{ij}^{B}\right)}{\sigma_{0}^{2}} + \frac{\left(\theta - \theta^{B}\right) \left(\theta - \theta^{B}\right)}{\theta_{0}^{2}} - 1$$
(8)

Note that the transformation strain is assumed to be isochoric and thus only the deviatoric part of the stress,  $s_{ij} = \sigma_{ij} - \frac{\delta_{ij}\sigma_{kk}}{3}$ , can drive the transformation. The material parameters  $\sigma_0$  and  $\theta_0$  set the sizes of the transformation surface in the stress and temperature directions, and these are closely related to the size of the hysteresis loops during stress or temperature cycling of the material. For states where  $\Phi < 0$  the material response is linear and there is no evolution of either the transformation strain or entropy. However, when  $\Phi = 0$  the transformation strain and entropy evolve according to an associated flow rule as,

$$\dot{\varepsilon}_{ij}^t = 3\lambda \frac{\left(s_{ij} - s_{ij}^B\right)}{\sigma_0^2} \tag{9}$$

$$\dot{s}^t = 2\lambda \frac{\left(\theta - \theta^B\right)}{\theta_0^2} \tag{10}$$

Here  $\lambda$  is a non-negative plastic multiplier. Note that if the load increment induces transformation strain or transformation entropy and the stress or temperature state is on the transformation surface then Eqs. (9) and (10) indicate that the transformation strain increment and transformation entropy increment are normal to the transformation surface.

As indicated in Eq. (1), the hardening potential is only a function of the internal variables  $\varepsilon_{ij}^t$  and  $s^t$ . The tension/compression asymmetry in the material behaviors is captured using the following construction of the transformation potential.

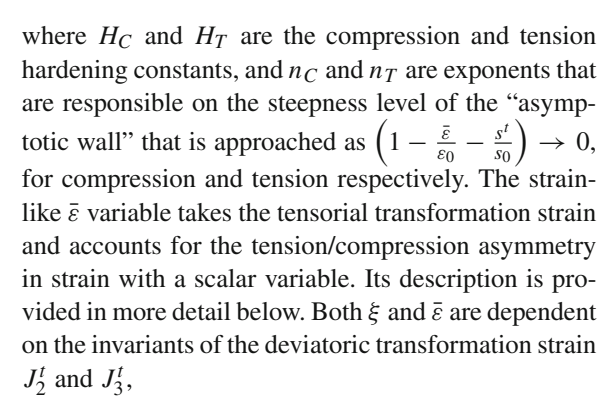
$$\Psi^{t} = \xi \Psi_{C}^{t}(J_{2}^{t}, \bar{\varepsilon}, s^{t}) + (1 - \xi)\Psi_{T}^{t}(J_{2}^{t}, \bar{\varepsilon}, s^{t}) 
+ \Psi_{s}(s^{t})$$
(11)

The functions that are used in Eq. (11) for describing the transformation potential for a material that hardens during transformation have the following forms

$$\Psi_T^t = \frac{1}{2} H_T J_2^{t^2} \frac{1}{\left(1 - \frac{\bar{\varepsilon}}{\varepsilon_0} - \frac{s^t}{s_0}\right)^{n_T}}$$
 (12)

$$\Psi_C^t = \frac{1}{2} H_C J_2^{t^2} \frac{1}{\left(1 - \frac{\bar{\varepsilon}}{\varepsilon_0} - \frac{s^t}{s_0}\right)^{n_C}}$$
 (13)

$$\Psi_{s} = H_{1}^{s} \frac{1}{\left(1 - \frac{s^{t}}{s_{0}}\right)^{u} \left(\frac{s^{t}}{s_{0}}\right)^{v}} + \theta^{t} s^{t} + \frac{1}{2} H_{2}^{s} s^{t^{2}}$$
 (14)



$$J_2^t = \left(\frac{2}{3}e_{ij}^t e_{ij}^t\right)^{\frac{1}{2}} \tag{15}$$

$$J_3^t = \left(\frac{4}{3}e_{ij}^t e_{jk}^t e_{ki}^t\right)^{\frac{1}{3}} \tag{16}$$

where  $\bar{\varepsilon}$  and  $\xi$  are defined as

$$\bar{\varepsilon} = J_2^t f(J_r) \tag{17}$$

$$\xi(J_r) = \frac{1 - J_r^3}{2} \tag{18}$$

with  $J_r = J_3^t/J_2^t$ , and in this work,

$$f = \cos\left[\frac{\cos^{-1}[1 - a(J_r^3 + 1)]}{3}\right]$$
 (19)

The material property  $\varepsilon_0$  is maximum amount of compressive strain that can be achieved by polycrystalline 100% martensite. The amount of strain that such a martensite phase can achieve in tension is  $\varepsilon_0/f(1)$ .

# 3 Steady state crack growth

Figure 1 shows a schematic of the boundary value problem being solved. Plane strain conditions are assumed for a semi-infinite crack growing with a crack tip speed of  $\dot{a}$  along the  $x_1$ -axis under mode I loading. The crack flanks are assumed to be traction-free and thermally insulated. The applied far field mechanical loading on the outer boundary consists of tractions that are consistent with the mode I K-field.

$$\sigma_{xx} = \frac{K_I}{\sqrt{2\pi r}} \cos \frac{\theta}{2} \left( 1 - \sin \frac{\theta}{2} \sin \frac{3\theta}{2} \right)$$

$$\sigma_{yy} = \frac{K_I}{\sqrt{2\pi r}} \cos \frac{\theta}{2} \left( 1 + \sin \frac{\theta}{2} \sin \frac{3\theta}{2} \right)$$

$$\sigma_{xy} = \frac{K_I}{\sqrt{2\pi r}} \left( \sin \frac{\theta}{2} \cos \frac{3\theta}{2} \cos \frac{3\theta}{2} \right)$$
(20)



Here r and  $\theta$  are a polar coordinate system centered on and fixed to the growing crack tip. Additionally, the initial temperature is homogeneous and the outer boundary is thermally insulated. The magnitude of the applied  $K_I$  is chosen such that the size of the transformation zone,  $R_t$ , near the crack tip is always less than 100 times the distance from the crack tip to the outer boundary. The apparent applied steady state energy release rate for the system is then related to  $K_I$  as,

$$G_{ss} = \frac{1 - v^2}{E} K_I^2 \tag{21}$$

This represents the amount of energy that is available both to drive the crack tip separation process, and for the energy dissipated in the bulk. The purpose of this work is to determine the energy available for the crack tip separation process and thus the toughening enhancement due to transformation. In addition to mechanical equilibrium,  $\sigma_{ji,j} = 0$ , the numerical calculations must also solve the heat equation resulting from an analysis of the first law shown in Eq. (4). Using the deviatoric nature of the transformation strain, the flow rule, and the transformation surface it can be shown that,

$$\dot{\Psi} = \sigma_{ij}\dot{\varepsilon}_{ij} - s\dot{\theta} + \frac{\partial\Psi}{\partial\varepsilon_{ij}^t}\dot{\varepsilon}_{ij}^t + \frac{\partial\Psi}{\partial s^t}\dot{s}^t$$

$$= \sigma_{ij}\dot{\varepsilon}_{ij} - s\dot{\theta} - 3\lambda \frac{\left(s_{ij} - s_{ij}^B\right)\left(s_{ij} - s_{ij}^B\right)}{\sigma_0^2}$$

$$-2\lambda \frac{\left(\theta - \theta^B\right)^2}{\theta_0^2} = \sigma_{ij}\dot{\varepsilon}_{ij} - s\dot{\theta} - 2\lambda \tag{22}$$

Applying this result into the first law in Eq. (4) leads to,

$$\theta \dot{s} = (k_{ij}\theta_{,i})_{,i} + r + 2\lambda \tag{23}$$

where again  $k_{ij}$  is the thermal conductivity tensor and  $\lambda$  is the plastic multiplier which interestingly in this theory is also half of the non-conduction part of the dissipation rate. The time derivative of the total entropy,  $\dot{s}$ , derived from Eq. (3) is then expressed as,

$$\dot{s} = C \frac{\dot{\theta}}{\theta} + \beta_{ij} \left( \dot{\varepsilon}_{ij} - \dot{\varepsilon}_{ij}^t \right) + \dot{s}^t \tag{24}$$

where *C* is the heat capacity. Therefore, the heat equation within this theoretical structure is expressed as,

$$C\dot{\theta} + \theta \beta_{ij} \left( \dot{\varepsilon}_{ij} - \dot{\varepsilon}_{ij}^t \right) + \theta \dot{s}^t = \left( k_{ij} \theta_{,j} \right)_{,i} + r + 2\lambda \tag{25}$$

Eq. (25) has several terms that warrant further explanation. The first term on the left-hand side is the standard heat storage due to the thermal capacity of the material. The second term is a thermoelastic heating term which is generally relatively small (in this work we will take  $\beta_{ij} = 0$ ). The third term represents the latent heat of transformation that is released when the material transforms from austenite to martensite. Note that during the austenite to martensite transition  $\dot{s}^t < 0$ and so the term  $\theta \dot{s}^t$  acts much like a heat source term (i.e. like a positive r on the right-hand side) causing the material to increase in temperature under isentropic conditions. The first term on the right-hand side is the standard Fourier conduction term and represents the amount of heat conducted into the point. Finally, the last term on the right-hand side represents the dissipation associated with the irreversible thermomechanical transformation behavior, which again acts like a heat source term.

Note that the time rates of change of several quantities appear throughout the heat equation, and this is the source of all of the rate dependence of the fracture behaviors explored in this work. There is no rate dependence inherent to the intrinsic constitutive behavior, but the mechanical material response is very sensitive to the rate at which the latent heat of transformation can be expelled from the material since this governs the temperature. For steady state crack growth conditions these time rates of change are converted to spatial derivatives, and then the problem is solved on a coordinate system attached to the moving crack tip. For any field quantity f with the crack moving in the  $x_1$  direction at a constant crack tip velocity of  $\dot{a}$ , the material time derivative of f is given as,

$$\frac{df}{dt} = -\dot{a}\frac{\partial f}{\partial x_1} \tag{26}$$

Along with Eq. (26), no external heat source r = 0, and the assumption that the thermoelastic coefficients  $\beta_{ij} = 0$ , the weak forms for mechanical equilibrium and the heat equation can be expressed as,

$$\int_{V} \delta \varepsilon_{ij} c_{ijkl} \varepsilon_{kl} dV 
= \int_{S} \delta u_{i} T_{i} dS + \int_{V} \delta \varepsilon_{ij} c_{ijkl} \varepsilon_{kl}^{t} dV 
\int_{V} \left( \delta \theta_{,i} k \delta_{ij} \theta_{,j} - \delta \theta C \dot{a} \theta_{,1} \right) dV 
= \int_{S} \delta \theta q_{i} n_{i} dS + \int_{V} \delta \theta \left( \dot{a} \theta s_{,1}^{t} + 2\lambda \right) dV$$
(28)

where V is the volume and S is the surface of the simulation domain, and  $T_i$  are the tractions applied on the boundary surface as  $T_i = \sigma_{ji} n_j$ , with the stresses given by Eq. (20). Also note that  $q_i n_i = 0$  on the outer insulated boundary and along all crack faces, so the first term on the right-hand side of Eq. (28) is zero.

With the application of standard finite element procedures, the left-hand side of Eq. (27) leads to a standard linear elastic stiffness matrix which needs to be inverted a single time and then stored. Similarly, the left-hand side of Eq. (28) leads to a linear heat conduction matrix with a standard symmetric part from the thermal conductivity and a non-symmetric part associated with the heat capacity and crack tip speed. Again, this constant matrix needs to be inverted only once and stored. The right-hand sides of Eqs. (27) and (28) represent unbalanced generalized forces. An iterative procedure is applied to drive these terms to zero. In the first iteration the initial transformation strain is assumed to be zero and the transformation entropy is taken to be consistent with the ambient temperature, close to  $s_0$ when in the austenite phase and close to zero when in the martensite phase. The temperature is initially assumed to be homogeneous at the specified ambient level. Updates to the nodal displacements and temperatures are then obtained by solving the system for the initially unbalanced generalized forces. Using these new approximations for the displacements and temperature, the strains are calculated based on the finite element interpolations and new approximations for the stresses, transformation strains, and transformation entropy are calculated by integrating the SMA constitutive model along streamlines of constant heights above the crack plane from the right edge of the simulation domain to the left. With these updated approximation for the transformation strain, transformation entropy, and temperature, the residual generalized forces are recalculated and new nodal displacements and temperatures are obtained. This process is repeated until a suitable level of convergence is achieved.

Once convergence is achieved, in addition to the distribution of the thermomechanical fields, the amount of energy available to drive material separation at the crack tip is also of interest. For steady crack growth Hutchinson's path-independent *I*-integral (Hutchinson 1974), can be used to calculate the crack tip energy release rate,

$$G_{\text{tip}} = I = \int_{\Gamma} \left( W n_1 - \sigma_{ij} n_j u_{i,1} \right) d\Gamma$$
 (29)



where  $\Gamma$  is a counterclockwise contour around the crack tip and  $n_i$  is the outward unit normal to the contour  $\Gamma$ . The work density W is path-dependent at a general material point and given as,

$$W = \int_0^{\varepsilon_{ij}} \sigma_{ij} d\varepsilon_{ij} \tag{30}$$

Note that for a general thermomechanical loading a "heat density" term would also be needed in the calculation of the energy release rate. However, in this problem both r=0 and the entire boundary of the simulation domain is insulated, and thus any heat input contribution to the energy release rate vanishes. This numerical approach was originally developed by Dean and Hutchinson (1980) to study the plastic fields during steady crack growth. It has also been used in conjunction with cohesive zone laws ahead of the crack tip to model elastic-plastic and rate-dependent fracture behaviors. Landis (2003), Baxevanis et al. (2014b), and others have applied it to study steady crack growth in smart materials.

In the calculations it is assumed that while the crack is growing  $G_{tip} = G_0$ , where  $G_0$  is the intrinsic fracture toughness of the material, i.e. the toughness that would be measured if transformation could be frozen out of the material and prohibited from occurring. The purpose of these calculations is to determine the toughening due to the dissipative effects of transformation. Such toughening is represented as the ratio of  $G_{ss}/G_{tip}$ and is different from the fracture toughness, which cannot be unambiguously predicted with this approach due to the possible dependencies of  $G_0$  on temperature, phase, etc. The calculations presented here will show how  $G_{ss}/G_{tip}$  depends on both intrinsic material properties like the maximum amount of transformation strain, and extrinsic quantities like the temperature and the crack speed.

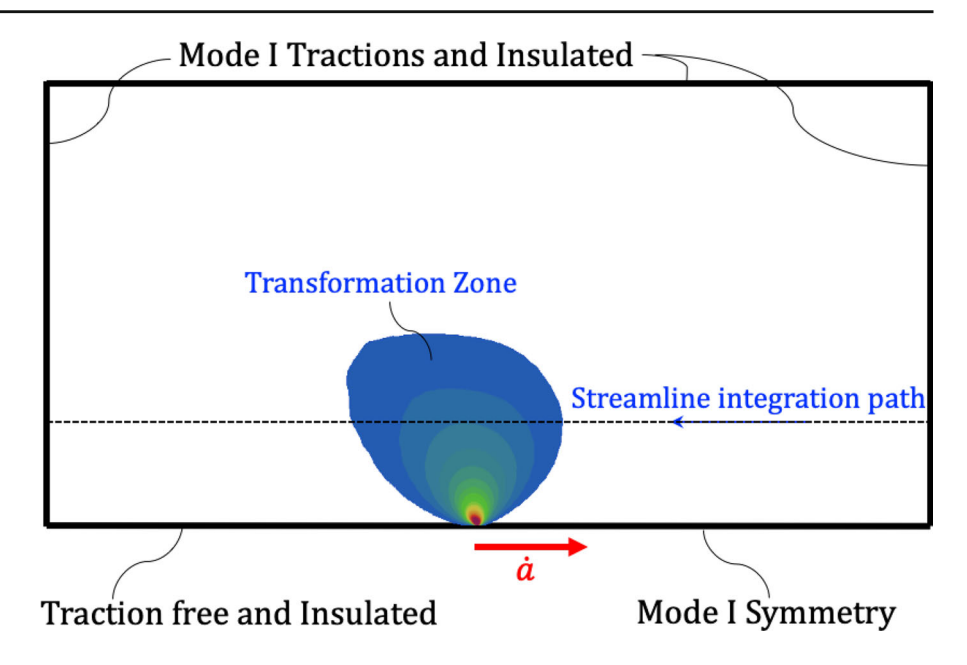
Dimensional analysis and manipulation of the constitutive model allows for the identification of the normalizations for strains  $(\varepsilon_{ij}/\varepsilon_0)$ , stresses  $(\sigma_{ij}/\sigma_0)$ , temperature  $(\theta/\theta_0)$  and entropy  $(s/s_0)$  which are fields that depend upon the normalized coordinates  $x_1/R_0$  and  $x_2/R_0$ . Here  $R_0$  is the characteristic size of the transformation zone for an applied stress intensity of

$$K_I = \sqrt{G_0 E/(1 - v^2)},$$

$$R_0 = \frac{1}{3\pi} \frac{G_0 E}{(1 - v^2) \sigma_0^2}$$
(31)

Note that the full size of the transformation zone,  $R_t$ , in any given calculation will scale with  $G_{ss}/G_0$  such

Fig. 1 A schematic of the steady-state crack growth problem illustrating the boundary conditions applied in the finite element calculations



that  $R_t = (G_{ss}/G_0)R_0$ . The field distributions, along with the toughening,  $G_{ss}/G_{tip}$ , are dependent on the following list of dimensionless groups,

$$\frac{\varepsilon_0 E}{\sigma_0}, \frac{H_T}{\sigma_0}, \frac{H_C}{\sigma_0}, \frac{\sigma_0 \varepsilon_0}{\theta_0 s_0}, n_T, n_C, \frac{\theta^t}{\theta_0}, \frac{s_0 H_2^s}{\theta_0}, \\
u, v, v, \frac{H_1^s}{s_0 \theta_0}; \frac{C}{s_0}, \frac{\dot{a} s_0 R_0}{k}, \frac{\theta}{\theta_0}$$
(32)

Here the semicolon separates the parameters that describe the SMA thermomechanical constitutive model that can be used to represent the range of isothermal behaviors (to the left), and those for the heat transfer properties which are required for either isentropic behavior or inhomogeneous temperature simulations (essentially the heat capacity and the thermal conductivity), and the applied temperature itself. In this work the most significant dimensionless parameters to be studied are the first three and the last three in Eq. (32). The parameter  $\varepsilon_0 E/\sigma_0$  can be thought of as either the ratio of the transformation strain  $\varepsilon_0$  to the elastic strain  $\sigma_0/E$ , or as the ratio of the dissipated energy  $\sigma_0\varepsilon_0$  to the stored energy  $\sigma_0^2/E$ . All of the prior work on toughening in smart materials has shown that the toughening is monotonically increasing with  $\varepsilon_0 E/\sigma_0$ . The next terms,  $H_T/\sigma_0$  and  $H_C/\sigma_0$  are the hardening in tension and compression, and again all of the prior work has shown that the toughening is monotonically decreasing with increasing hardening parameters. In essence, these two features show that stiffer and less dissipative materials show less toughening. The last two terms are

of more significant interest in this work as there is less prior work on their effects in the literature. However, it is possible to predict the expected trends in the toughening with respect to these parameters based on the idea that any feature that drives the material towards the high temperature austenite phase will have lower toughening than a situation where the transformation to martensite is more favorable. Considering materials beginning in the austenite phase, higher temperature  $\theta/\theta_0$  drives the material towards austenite and thus the toughening down. The ratio  $C/s_0$  relates the ability of the material to store heat to its ability to expel latent heat during the transformation. The higher this ratio is the lower the temperature change will be during isentropic transformation and thus the toughening should increase as  $C/s_0$  increases. Finally,  $\dot{a}s_0R_0/k$  is a ratio of how quickly the material expels heat during crack growth to how quickly the material can conduct heat away from the crack tip. In this case lower values of  $\dot{a}s_0R_0/k$ , i.e. very slow crack growth or very high thermal conductivity, will keep the temperature low near the crack tip and thus increase the toughening, while higher crack speeds will decrease the toughening.

# 4 Results

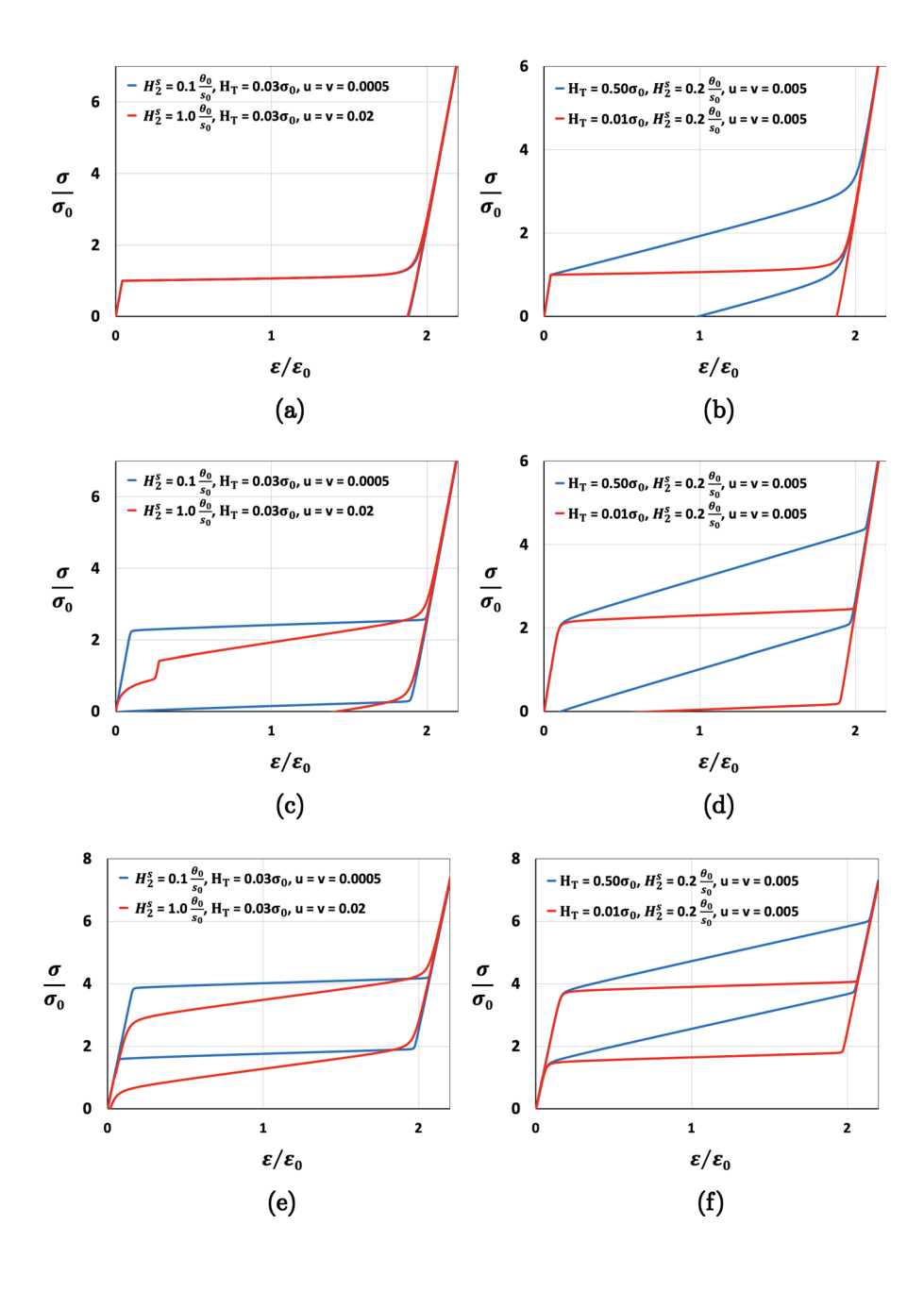
Prior to presenting the results for the steady crack growth simulations for different material properties



and crack speeds, the impact of the material properties presented in Eq. (32) on the stress-strain response in a uniaxial tension test at different temperatures is illustrated. The material parameter  $\theta^t$  controls the transition temperatures between martensite and austenite. The parameter  $H_T$  controls the hardening slope during stress-induced phase transformation and low temperature martensite detwinning process in uniaxial tension, and  $H_2^s$  controls the slope of the shallow-sloped "plateau" portion of the  $\theta^B-s^t$  response shown in Fig. 3 which sets the levels of the martensite-austenite start/finish temperatures and also affects the slopes of the shallow-sloped "plateau" portion of the uniaxial hardening behavior of the stress-induced austenite to martensite transition. Figure 2 shows the influence of these two parameters on the uniaxial tension tests. The exponents  $n_T$  and  $n_C$  control the approach to saturation and have a very mild effect on the stress-strain behaviors for the range of 0.01 to 0.7. The curvatures of the corners at the transitions between the asymptotes and

Fig. 2 Uniaxial tension  $\sigma$ - $\varepsilon$  response for a range of tension hardening constants  $H_T$  and different martensite/austenite start and finish temperatures  $H_2^s$ for the following material temperatures: a, b

 $\theta = 20.3\theta_0$ , c, d  $\theta = 25.3\theta_0$ , **e**, **f**  $\theta = 28.3\theta_0$ 





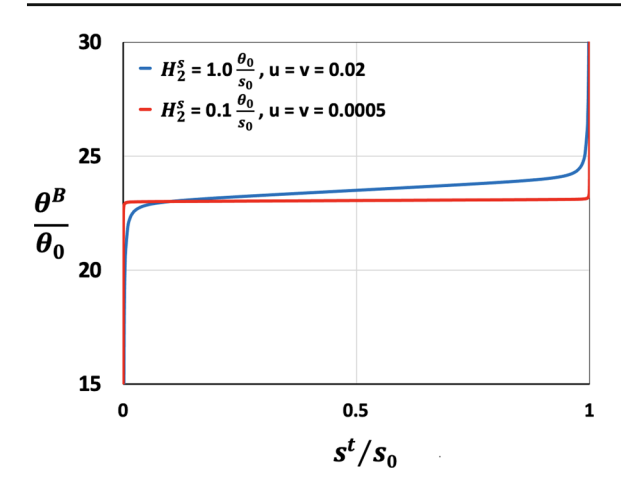


Fig. 3 The back temperature versus the transformation entropy derived from Eq. (14) for different martensite to austenite temperature slope  $H_2^s$ 

the shallow-sloped plateau region of the transformation entropy-back temperature curve shown in Fig. 3 are controlled by the parameters u and v, with smaller values leading to sharper corners at the transitions.  $H_1^s$  is a thermal modulus that controls the steepness of the asymptotes as  $s^t \to 0$  and  $s^t \to s_0$ . Additionally, v is the Poisson's ratio which for this work is taken to be 0.4 for both austenite and martensite.

Figure 2a and b illustrates the uniaxial stress-strain behaviors at a constant temperature of  $20.3\theta_0$  for different values of (a)  $H_2^s$ , u and v at  $H_T = 0.03\sigma_0$ and (b)  $H_T$  at  $H_2^s = 0.2\theta_0/s_0$ , u = v = 0.005. At this temperature the material is in the martensite phase, and as a result of cooling from the high temperature austenite phase, begins in a twinned martensite state with zero transformation strain. In this case, the transformation stress level is dictated by the parameters of the transformation surface at a uniaxial stress level of  $\sigma_0$ . As the transformation strain approaches the saturation strain of the pure martensite phase in tension  $\varepsilon_0/f(1)$ , the stress increases precipitously. Upon unloading and returning to zero stress, the transformation strain remains and the material is left in a detwinned martensite state. Here higher values of  $H_2^s$ have no impact on the uniaxial stress-strain response and higher values of  $H_T$  produce higher stress levels as transformation proceeds.

Figure 2c and d illustrates the uniaxial stress-strain behaviors at a constant temperature of  $25.3\theta_0$  for different values of (c)  $H_2^s$  at  $H_T = 0.03\sigma_0$  and (d)  $H_T$  at  $H_2^s = 0.2\theta_0/s_0$ , u = v = 0.005. This temperature is

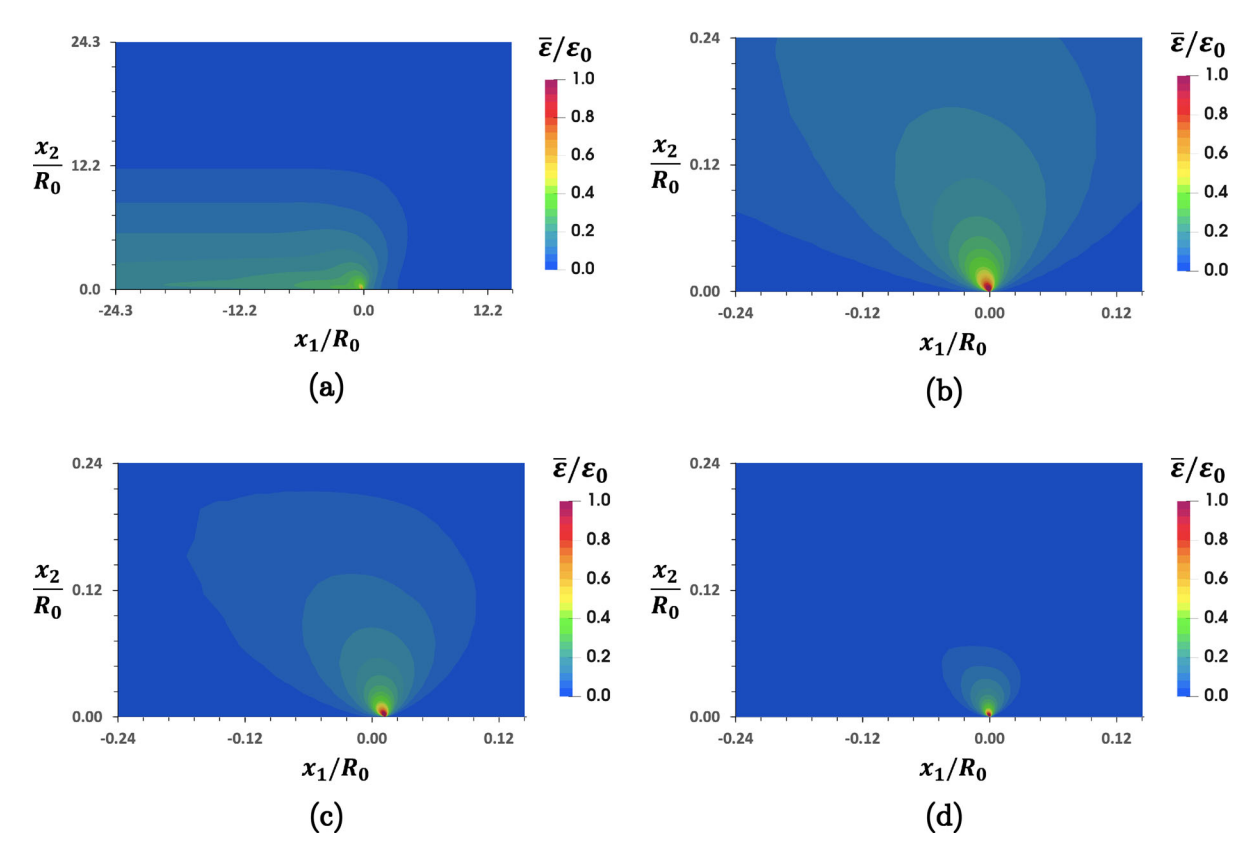
not significantly higher than the martensite to austenite finish temperature and the material begins in the austenite phase. Notice in this case that the transformation stress level is at approximately  $2\sigma_0$ , which shows that this strength is not solely defined by the parameters of the transformation surface as it was in the previous case for the martensite phase. Here, the increase in the transformation stress is due to the effects of the hardening potential that creates a rapidly rising back stress for very small but non-zero accumulations of the transformation strain that do occur when the applied stress is higher than  $\sigma_0$ . Hence, even though transformation is occurring in the mathematical model at uniaxial stress levels above  $\sigma_0$ , the apparent behavior remains elastic. In contrast to the uniaxial stress-strain responses in Fig. 2a and b, the plateau in Fig. 2c and d is driven by the stress-induced forward phase transformation as opposed to martensite detwinning. However, the saturation level of the transformation strain remains at  $\varepsilon_0/f(1)$  for high stress levels where the material is in a state of detwinned martensite.

Figure 2e and f illustrates the uniaxial stress-strain behaviors at constant temperature of  $28.3\theta_0$  for different values of (e)  $H_2^s$  at  $H_T=0.03\sigma_0$  and (f)  $H_T$  at  $H_2^s=0.2\theta_0/s_0$ , u=v=0.005. At this temperature, the description and features of the stress-strain behavior mimic those provided for Fig. 2c and d at the temperature of  $25.3\theta_0$ . The difference being that the transformation stress levels for forward and reverse transformation occur at considerably higher values than those at  $25.3\theta_0$ . This behavior is an example of the competition between the stress driving the material towards the detwinned martensite phase and the temperature driving the material towards the austenite phase that is encoded within the functional forms of the hardening potential.

As shown in Fig. 1 the analysis of the steady crack growth problem is performed on the upper half plane due to the assumption of mode I symmetry. The finite element mesh is refined near the crack tip in order to capture the details of the non-linear transformation zone. Mode I symmetry boundary conditions are applied ahead of the crack tip and traction free and insulating conditions are applied on the crack faces. Mode I tractions and insulating conditions are applied on the remote outer boundary. The initial temperature distribution is homogeneous throughout the domain.

To gain an understanding of how the behavior depends on the ambient temperature, Fig. 4 shows con-





**Fig. 4** The distribution of transformation strain,  $\bar{\epsilon}$ , close to the steadily growing crack for a range of initial material temperatures: **a**  $\theta = 20.3\theta_0$ ,  $G_{ss}/G_{tip} = 31.15$ , **b**  $\theta = 25.3\theta_0$ ,  $G_{ss}/G_{tip} = 3.64$ , **c**  $\theta = 26.8\theta_0$ ,  $G_{ss}/G_{tip} = 2.42$ , **d**  $\theta = 29.8\theta_0$ ,  $G_{ss}/G_{tip} = 1.53$ . The material and conductivity prop-

erties used for those numerical solutions are  $\varepsilon_0 E/\sigma_0 = 24$ ,  $\sigma_0 \varepsilon_0/s_0 \theta_0 = 0.981$ ,  $H_T = 0.2 \sigma_0$ ,  $H_C = 8 H_T$ ,  $n_T = 0.05$ ,  $n_C = 0.1$ ,  $H_1^s = 0.5 \theta_0 s_0$ ,  $\theta^t = 23 \theta_0$ ,  $H_2^s = 0.2 \theta_0/s_0$ ,  $\nu = 0.3$ ;  $C = 5 s_0$ ,  $\dot{a} s_0 R_0/k = 8$ 

tours of the effective transformation strain,  $\bar{\varepsilon}$ , in the vicinity of the crack tip for different initial temperatures. Figure 4b, c, and d is for temperatures where the material is in the austenite phase and illustrate the tendency of the material to reverse transform once the crack tip passes by. In contrast, Fig. 4a is at a temperature of  $20.3\theta_0$  which places the material in the martensite phase and there is a permanent wake of transformed material behind the crack tip for this case. This is a common feature for steady crack growth in elasticplastic materials and in ferroelastic materials. As the area around the crack tip is approached by a point just above the crack plane, the material goes through different deformation regimes. (i) Before entering the transformation zone near the crack tip, there is no phase transformation and the material resides in a twinned martensite state with zero macroscopic transformation strain. (ii) Entering the transformation zone the material state evolves from twinned martensite to detwinned martensite. As the point passes over and around the crack tip the principle directions of the transformation strain can and do rotate. We refer to this as transformation strain reorientation, and as with the initial detwinning this behavior is also associated with dissipation of energy (i.e. the plastic multiplier  $\lambda \neq 0$ ). (iii) Once the crack tip is passed over, the material experiences unloading from the detwinned and reoriented martensite state and a wake of transformation strain is left behind the crack tip.

In contrast, Fig. 4b, c, d shows the transformation strain contours for a material at initial temperatures of  $25.3\theta_0$ ,  $26.8\theta_0$  and  $29.8\theta_0$  respectively, each of which puts the material in the austenite phase initially. When comparing the relative sizes of the transformation zones for these three cases it is important to note that the transformation zone size  $R_t$  is proportional to the steady



state energy release rate  $G_{ss}$ , and so the absolute size of the transformation zone is largest for  $\theta = 25.3\theta_0$ and smallest for  $\theta = 29.8\theta_0$ . Again, as the area around the crack tip is approached from a point just above the crack plane, the material goes through different regimes of deformation behavior. (i) Before entering the transformation zone there is no phase transformation and the material starts in austenite state at transformation strain of zero and a transformation entropy of  $s_t \approx s_0$ . (ii) Entering the transformation zone the high stresses near the crack tip cause the stress induced phase transformation from austenite to martensite. The transformation strain increases and the transformation entropy decreases. (iii) As the point passes above and around the crack tip the principal directions of the transformation strain can reorient. Points sufficiently close to the crack tip will reside in a fully saturated transformation strain state but can still experience strain reorientation. For such points the transformation entropy  $s_t$  is approximately zero. (iv) As the crack tip is passed by the elevated stresses near the crack tip are no longer present to maintain the strained martensite state and the material experiences reverse transformation. Sufficiently far from the crack tip there is a complete reversal of the phase transformation with the material returning to its original austenite state and no wake of transformation strain left behind. Even without a wake of transformation strain there is still energy dissipated during this process and this energy dissipation leads to fracture toughening.

Note that these calculations do not incorporate plasticity into the constitutive law and thus for points close to the crack tip, the stresses increase severely within a small zone where strain saturation occurs. As for ferroelastic materials (Landis 2003), the numerical results suggest that the behavior of stresses near the crack tip behave as  $1/\sqrt{r}$ . However, adding plasticity to the calculations would introduce a very small plastic zone near the crack tip which would alter this type of behavior.

Figure 5a–d shows the temperature contours corresponding to the transformation strain contours in Fig. 4a–d. Note that these simulations use  $C=5s_0$  which is characteristic of NiTi, and a crack speed of  $\dot{a}=8k/s_0R_0$ , which is on the order of centimeters per second for properties relevant to NiTi. Here we have taken  $R_0\approx 1$  cm based on the work of Haghgouyan et al. (2019). In Fig. 5a, when  $\theta=20.3\theta_0$  shows that the temperature change in the vicinity of the crack tip is very small. Note that the temperature scale has a very

small range in order to produce the color contours that are displayed. This is due to the fact that there is no phase transformation from austenite to martensite in this case.

The material begins in the martensite phase and remains in the martensite phase throughout and hence there is no latent heat of transformation being released. There is detwinning and strain reorientation which are accompanied by a modest amount of dissipation and heat generation, but not to the levels seen in the cases where latent heat is released. Figure 5b, c, and d shows a common shape of the temperature profile, with the size of the affected region scaling with the transformation zone size and thus the level of the steady state energy release rate  $G_{ss}$ . As should be expected the maximum latent heat release is achieved near the crack tip where the stresses drive a complete transformation from austenite to martensite. The temperature decreases farther from the crack tip but the affected region is larger than the transformation zone due to the conduction of heat away from the elevated temperature region near the crack tip.

The remainder of this section includes results for the amount of toughening,  $G_{ss}/G_0$ , as a function of dimensionless combinations of material parameters  $\varepsilon_0 E/\sigma_0$ ,  $H_T/\sigma_0$ , and  $C_0/s_0$ , as well as the normalized crack speed to thermal conductivity ratio  $\dot{a}s_0R_0/k$  at different temperatures  $\theta/\theta_0$ . Figure 6a–c shows the ratio  $G_{ss}/G_0$ versus  $\varepsilon_0 E/\sigma_0$ , for a range of initial normalized temperatures  $\theta/\theta_0$ . The parameters used are identical to those used in Fig. 4 but with a slower crack speed of  $\dot{a}s_0R_0/k = 1$ . Figure 6a is for a material at an initial ambient temperature of  $27.8\theta_0$ . Here the material begins in the austenite phase. The results confirm the expectation that the amount of toughening,  $G_{ss}/G_{tip}$ , increases as the ratio  $\varepsilon_0 E/\sigma_0$  increases. This result is in line with prior studies and shows that increasing the propensity of the material for energy dissipation versus energy storage produces higher amounts of toughening.

Figure 6b plots the toughening as a function of  $\varepsilon_0 E/\sigma_0$  for ambient temperature of  $25.8\theta_0$  and Fig. 6c plots the same for ambient temperatures of  $10.0\theta_0$  and  $20.3\theta_0$  (both curves lie on top of one another). In Fig. 6b the ambient temperature is close to the martensite to austenite transition temperature and in Fig. 6c the material is in the martensite phase. Figure 6b shows a very similar behavior to Fig. 6a but with a higher toughening level as a function of  $\varepsilon_0 E/\sigma_0$ . Again, this can be expected based on the lower temperature than that



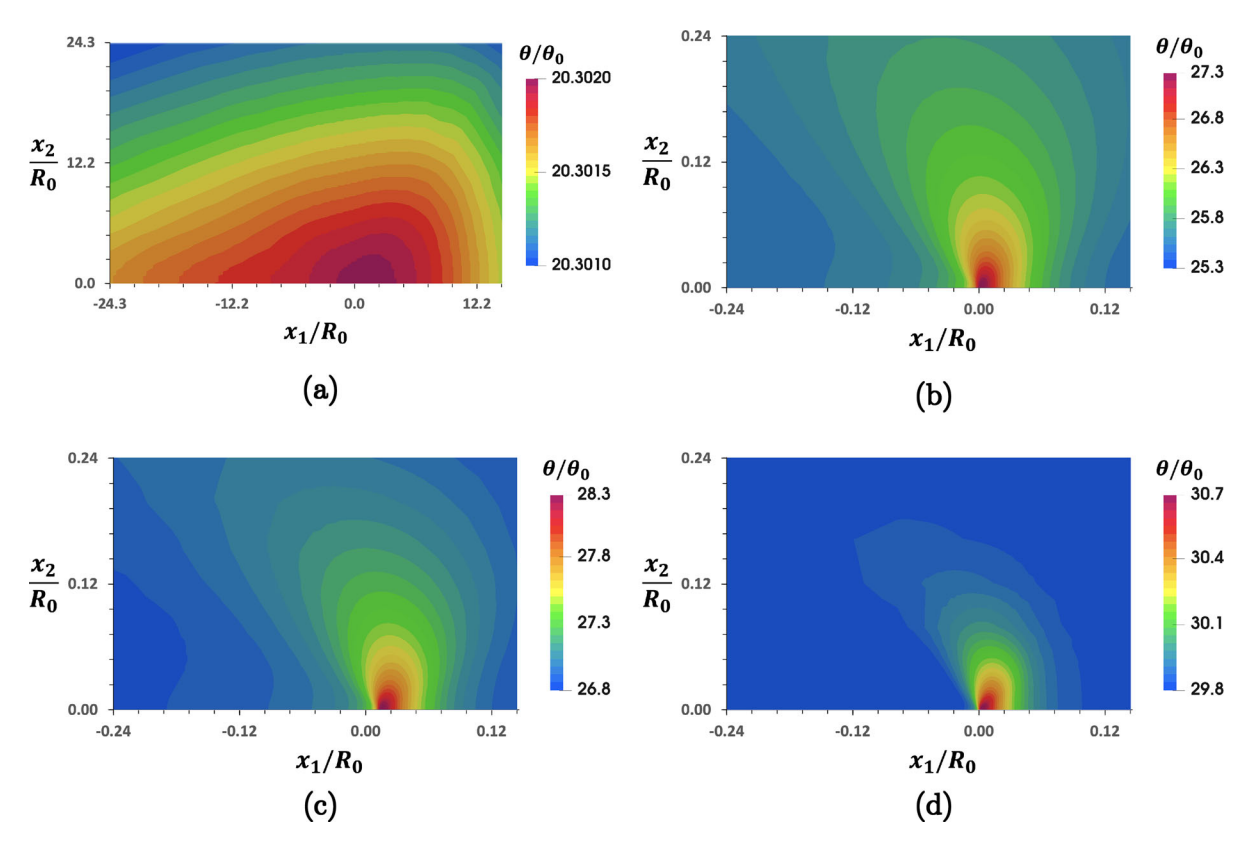


**Fig. 5** The distribution of the temperature,  $\theta/\theta_0$ , close to the steadily growing crack for a range of initial material temperatures:  $\mathbf{a} \ \theta = 20.3\theta_0, \ G_{ss}/G_{tip} = 31.15, \ \mathbf{b} \ \theta = 25.3\theta_0, \ G_{ss}/G_{tip} = 3.64, \ \mathbf{c} \ \theta = 26.8\theta_0, \ G_{ss}/G_{tip} = 2.42, \ \mathbf{d} \ \theta = 29.8\theta_0, \ G_{ss}/G_{tip} = 1.53$ . The material and conductivity prop-

erties used for those numerical solutions are  $\varepsilon_0 E/\sigma_0 = 24$ ,  $\sigma_0 \varepsilon_0/s_0 \theta_0 = 0.981$ ,  $H_T = 0.2\sigma_0$ ,  $H_C = 8H_T$ ,  $n_T = 0.05$ ,  $n_C = 0.1$ ,  $H_1^s = 0.5\theta_0 s_0$ ,  $\theta^t = 23\theta_0$ ,  $H_2^s = 0.2\theta_0/s_0$ ,  $\nu = 0.3$ , u = 0.005, v = 0.0005;  $C = 5s_0$ ,  $\dot{a}s_0 R_0/k = 8$ 

in the case shown in Fig. 6a. The lower temperature stimulates the transition from austenite to martensite which is the source of the toughening. Aside from the increasing dependence of the toughening on  $\varepsilon_0 E/\sigma_0$ , Fig. 6c shows some distinct differences in behavior to that seen in Fig. 6a and b. First, the temperature dependence of the toughening has vanished. At these temperatures the material is in the martensite phase and the toughness enhancement is purely due to the detwinning and reorientation of martensite. Essentially identical behavior is seen for ferroelastic ceramics, Landis (2003), as the constitutive behavior can be described with a similar model. In contrast to the temperatures where austenite is stable and reverse transformation does not allow for a wake of transformed material, the low temperature martensite phase does not reverse transform upon unloading and does leave behind a transformation wake. Additionally, the relatively low transformation stress for the pure martensite phase

leads to a much larger transformation zone where the dissipative effects of martensite detwinning and reorientation appear. Here, a simple back-of-the-envelope dimensional calculation is informative. The size of the transformation zone can be approximated as  $R_t \approx$  $G_{ss}E/(\alpha_t\sigma_0)^2$ , where  $\alpha_t\sigma_0$  is an effective transformation stress, i.e. the upper plateau level for the stressstrain curves shown in Fig. 2. For ambient temperatures where the austenite phase is stable  $\alpha_t > 1$  and increases with increasing temperature. For ambient temperatures in the martensite phase  $\alpha_t = 1$ . The amount of energy dissipated in the transformation zone is approximately  $W_{dis} \approx c\sigma_0 \varepsilon_0$ . Here a constant c has been introduced to account for the many approximations being made, and would incorporate other parameters like the hardening moduli. The steady state toughness can then be approximated as  $G_{ss} \approx W_{dis}R_t + G_0$ , which to first order in  $\varepsilon_0 E/\sigma_0$  yields,  $G_{ss} \approx G_0(1+c\varepsilon_0 E/\alpha_t^2\sigma_0)$ . What this formula indicates is that for temperatures where



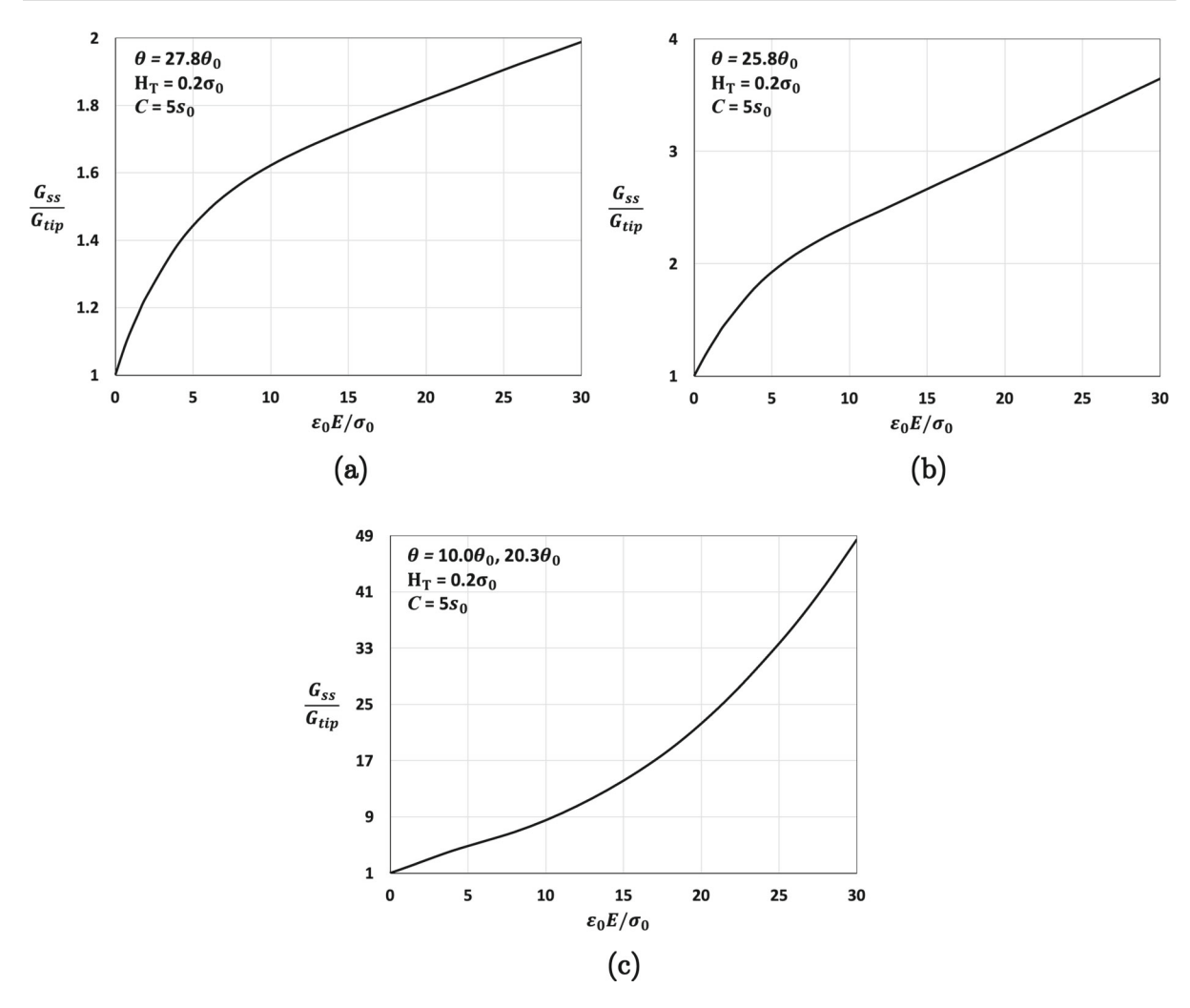


Fig. 6 The toughening amount,  $G_{ss}/G_{tip}$ , under steady state crack growth as a function of  $\varepsilon_0 E/\sigma_0$ , for different initial normalized temperatures:  $\mathbf{a} \theta = 27.8\theta_0$ ,  $\mathbf{b} \theta = 25.8\theta_0$ ,  $\mathbf{c} \theta = 10.0\theta_0$  and  $\theta = 20.3\theta_0$ 

martensite is stable, the temperature dependence of the toughening should be very weak since  $\alpha_t$  will remain at 1. In fact, this is what is seen in the calculations shown in Fig. 6c, where both sets of low temperature simulations show essentially identical toughening behavior as a function of  $\varepsilon_0 E/\sigma_0$ . However, for the austenite phase  $\alpha_t$  increases with temperature, for example  $\alpha_t=2.4$  for  $\theta=25.8\theta_0$  and  $\alpha_t=3.4$  for  $\theta=27.8\theta_0$ . Thus the simple formula that has just been derived for the toughening suggests that the initial slope of the  $G_{ss}/G_0$  versus  $\varepsilon_0 E/\sigma_0$  curve for  $\theta=25.8\theta_0$  should be  $(3.4/2.4)^2=2$  times that for  $\theta=27.8\theta_0$ . In fact, the ratio of the initial slopes of the toughening curves of Fig. 6a and b is indeed 2. Hence, this simple model can provide qualita-

tive and, to a limited extent, quantitative interpretations of the toughening behaviors seen in SMAs.

The next set of numerical simulations displayed in Fig. 7a and b shows the toughening ratio  $G_{ss}/G_{tip}$  versus the initial ambient temperature  $\theta/\theta_0$ , for a range of  $H_T/\sigma_0$  and  $H_2^s/\sigma_0$  values. The material parameters used in these numerical simulations are those listed in Fig. 4 but with a normalized crack speed of  $\dot{a}s_0R_0/k=1$ . Again note that as the ambient temperature increases the stress required for the forward transformation to occur increases and thus the size of the transformation zone near the crack tip decreases. These behaviors are represented in the uniaxial stress-strain responses shown in Fig. 2c–f, and in the transformation strain contours shown in Fig. 4b–d. As expected,



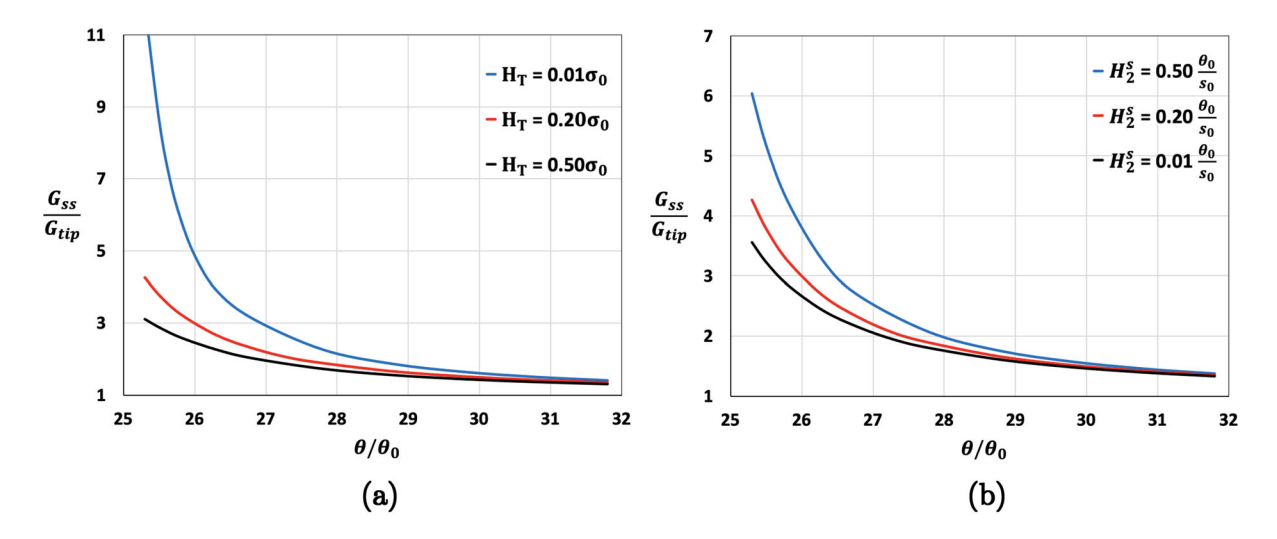


Fig. 7 The toughening amount,  $G_{ss}/G_{tip}$ , under steady state crack growth as a function of normalized temperature,  $\theta/\theta_0$ , for **a** various values of the tensile hardening parameter,  $H_T$ , at  $H_2^s = 0.2\theta_0/s_0$  and **b** various values of the slope of the martensite to austenite transition temperature,  $H_2^s$ , at  $H_T = 0.2\sigma_0$ . The

material and conductivity properties used for those numerical solutions are  $\varepsilon_0 E/\sigma_0 = 24$ ,  $\sigma_0 \varepsilon_0/s_0 \theta_0 = 0.981$ ,  $H_C = 8H_T$ ,  $n_T = 0.05$ ,  $n_C = 0.1$ ,  $\theta^I = 23\theta_0$ , u = 0.005, v = 0.0005;  $C = 5s_0$ ,  $\dot{a}s_0 R_0/k = 1$ 

as the ambient temperature drives the material towards the austenite phase Fig. 7 shows that the toughening decreases.

Figure 7a also illustrates the effects of the hardening parameter  $H_T/\sigma_0$ . Here the sensitivity of the toughening to the level of  $H_T/\sigma_0$  is small for high ambient temperatures and becomes significant as the initial ambient temperature of the material approaches the austenite to martensite transition temperature. This result indicates that softer materials show an enhancement of the toughening over high hardening materials. This is again in line with the expectation that stronger/harder materials show less toughening due to the distribution of the transformation strain near the crack tip and overall smaller amount of dissipation in that region. Figure 2d, f illustrates that increasing the values of  $H_T/\sigma_0$  produces steeper stress-strain slopes during the forward and reverse transformations, which increases the transformation stress level required for the phase transformation to proceed. Therefore, higher levels of  $H_T/\sigma_0$ restrict the full phase transformation to smaller areas around the crack tip resulting in a lower toughness enhancement.

Figure 7b shows the effect of the  $H_2^s$  parameter, which controls the slope of the back temperature-transformation entropy curve for the martensite to austenite transition, on the level of toughening. Again, the sensitivity of the toughness enhancement to changes

in  $H_2^s$  is small for high temperatures and increases as the ambient temperature of the material approaches the austenite to martensite transition temperature. Figure 2c, e illustrates a mixed effect of  $H_2^s$  on the initial transformation stress and the hardening during transformation, with the initial stress decreasing but the hardening increasing. Ultimately the detailed calculations confirm the intuition provided by the simple model that predicts that the lower initial transformation stress induced by higher values of  $H_2^s$  leads to an effectively larger transformation zone and a greater toughness enhancement.

The final sets of simulations presented here focus on the effects of the thermal properties on the toughness enhancement for ambient temperature ranges where the material is in the austenite phase. Recall that slow crack speeds,  $\dot{a}$ , and higher levels of thermal conduction, k, act to alleviate the temperature elevation that can occur due to the release of the latent heat during the transformation from austenite to martensite. Additionally, a higher heat capacity, C, will allow for more latent heat release without as large an isentropic increase in temperature. These considerations suggest that the toughness enhancement will be greatest for slow crack speeds, higher thermal conduction, and higher heat capacity.

Figure 8a and b illustrates the steady-state toughness enhancement as a function of the normalized crack



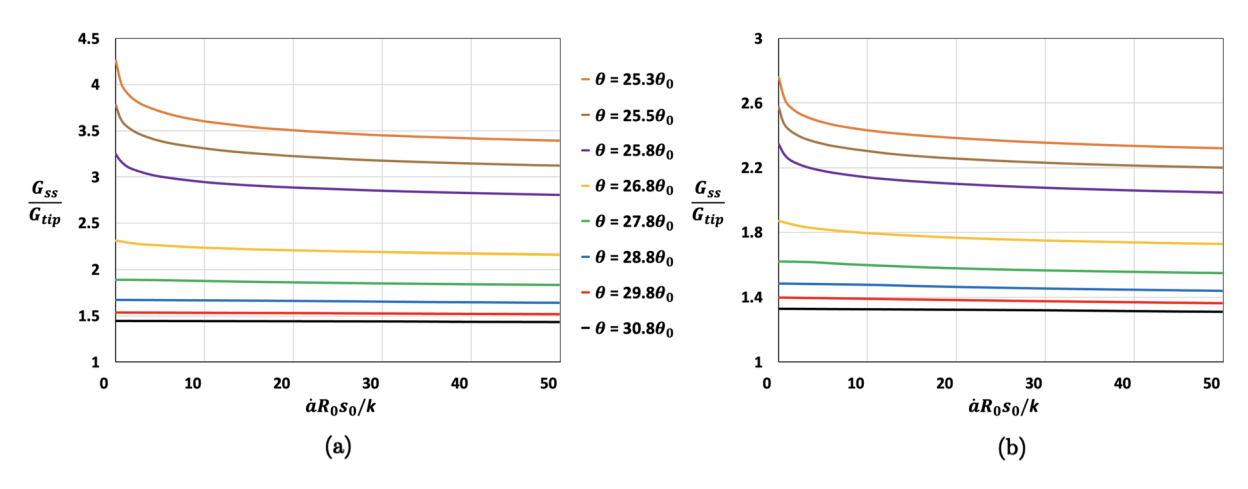


**Fig. 8** The toughness enhancement,  $G_{ss}/G_{tip}$ , under steady state crack growth as a function of normalized crack speed,  $\dot{a}s_0R_0/k$ , for various values of normalized temperature,  $\theta/\theta_0$ , and for the ratio levels: **a**  $\varepsilon_0E/\sigma_0=24$ , **b**  $\varepsilon_0E/\sigma_0=10$ . The

material and conductivity properties used for those numerical solutions are  $\sigma_0 \varepsilon_0 / s_0 \theta_0 = 0.981$ ,  $H_T = 0.2 \sigma_0$ ,  $H_C = 8 H_T$ ,  $n_T = 0.05$ ,  $n_C = 0.1$ ,  $\theta^I = 23\theta_0$ ,  $H_2^s = 0.2\theta_0 / s_0$ , u = 0.005, v = 0.0005;  $C = 5s_0$ 

growth speed,  $\dot{a}R_0s_0/k$  for different values of normalized temperature,  $\theta/\theta_0$ , at values for (a)  $\varepsilon_0 E/\sigma_0 = 24$ and (b)  $\varepsilon_0 E/\sigma_0 = 10$ . The other material properties of interest are reported in the figure captions. Again, slower crack speeds allow more time for the latent heat generated to diffuse away from the crack tip which keeps the local crack tip temperature close to that of the sample temperature and thus increases the toughening. In contrast, fast crack speeds do not allow time for the diffusion of heat and thus the local crack tip temperature increases and the local transformation stress increases as well, which in turn decreases the toughness enhancement. In the limit of very fast crack speeds or very slow heat conduction, the toughening will approach the isentropic limit for the associated ambient temperature. Note that the toughening is greater for the larger value of  $\varepsilon_0 E/\sigma_0 = 24$  in (a) than that for  $\varepsilon_0 E/\sigma_0 = 10$  in (b) for all temperature/crack-speed combinations.

Finally, Figure 9a and b presents the results for the steady-state fracture toughness enhancement versus the normalized crack speed for different values of heat capacity,  $C/s_0$ , for (a)  $\varepsilon_0 E/\sigma_0 = 24$  and (b)  $\varepsilon_0 E/\sigma_0 = 10$ . These figures summarize the effects of the thermal properties on the toughness enhancement. The latent heat of transformation for this material is approximately  $23s_0\theta_0$ , which is the plateau level of the temperature shown in Fig. 3 multiplied by the transformation entropy  $s_0$ . When interpreting the effects of crack speed one notes that faster crack growth drives the toughness down towards its isentropic value due to the

elevated temperature near the crack tip, which increases the transformation stress and decreases the toughening. The magnitude of the isentropic increase in temperature is governed by the ratio of  $C/s_0$ . According to Eq. (25) the isentropic temperature change is approximately,  $\Delta\theta \approx 23\theta_0s_0/C$ . Hence, greater values of the heat capacity C reduced the temperature change near the crack tip, keeping the transformation stress lower, and increasing the transformation zone dissipation and toughening. As with Fig. 8, the toughness enhancement for  $\varepsilon_0 E/\sigma_0 = 24$  in (a) is greater than that for  $\varepsilon_0 E/\sigma_0 = 10$  in (b) for all crack-speed/heat capacity combinations.

## 5 Discussion

In this work, the steady-state fracture toughness enhancement was studied using a phenomenological constitutive law for the thermomechanical behavior of SMAs, (Alsawalhi and Landis 2021). This constitutive model accounts for the forward and reverse phase transformations and the reorientation and detwinning of martensite, all using a single transformation surface and associated flow rule. Most all of the interesting behaviors associated with SMA behavior are accounted for using an energetic transformation potential formulated in terms of the transformation strain and transformation entropy internal variables. The interested reader is referred to Alsawalhi and Landis (2021) for additional details of the constitutive model. In contrast to previous



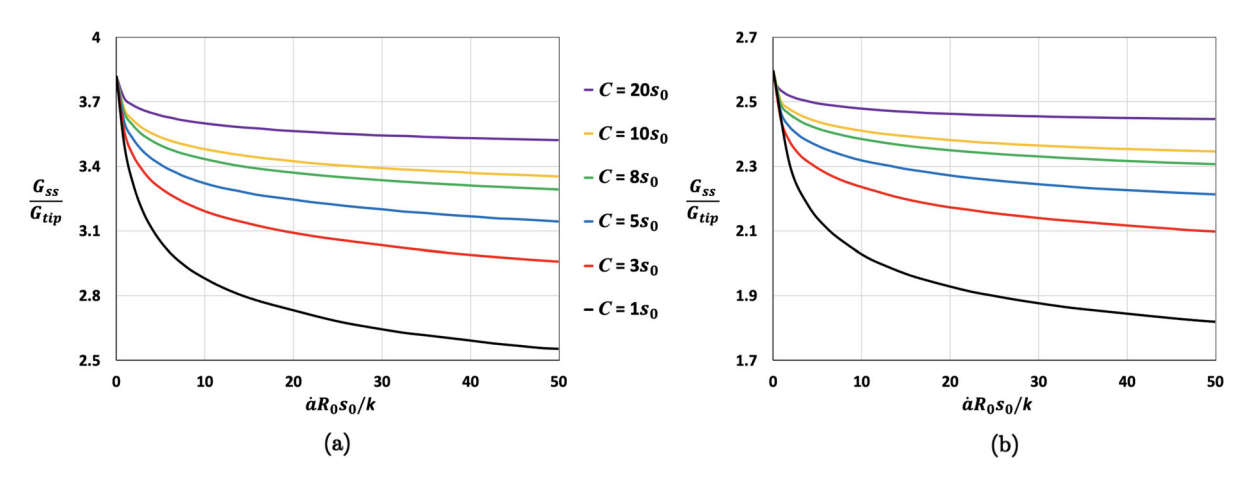


**Fig. 9** The toughness enhancement,  $G_{ss}/G_{tip}$ , under steady state crack growth as a function of normalized crack speed,  $\dot{a}s_0R_0/k$ , for various values of normalized heat capacity,  $C/s_0$ , and for the ratio levels: **a**  $\varepsilon_0E/\sigma_0 = 24$ , **b**  $\varepsilon_0E/\sigma_0 = 10$ . The

material and conductivity properties used for those numerical solutions are  $\sigma_0 \varepsilon_0 / s_0 \theta_0 = 0.981$ ,  $H_T = 0.2 \sigma_0$ ,  $H_C = 8 H_T$ ,  $n_T = 0.05$ ,  $n_C = 0.1$ ,  $\theta^I = 23\theta_0$ ,  $H_2^s = 0.2\theta_0 / s_0$ , u = 0.005, v = 0.0005;  $\theta = 25.5\theta_0$ 

studies on the steady-state toughening of SMAs, Baxevanis et al. (2014a,b), which looked at the isothermal and isentropic limits, this work investigated the non-isothermal behavior and the effects of crack speed on the toughening behavior. Hence, in addition to the governing equilibrium equations for the stress, the specialized steady-state finite element method also solved the heat equation governing the temperature field. One novel aspect of this work included the derivation of two "heat source" terms of interest for SMAs, and to the particular constitutive model used. Specifically, the latent heating rate term  $\theta \dot{s}^t$  appears in the heat equation as a source term during the transformation from austenite to martensite,  $\dot{s}^t < 0$ . This heat is then given back to the transformed material upon reverse transformation back to austenite  $\dot{s}^t > 0$ . Additionally, the dissipation rate due to phase transformation and martensite deformation also appears as a "source" term in the heat equation, specifically as twice the plastic multiplier,  $\dot{W}_{dis} = 2\lambda$ . This term is always positive as the plastic multiplier is constrained to be greater than or equal to zero.

The results for the toughening behavior predicted in this work can, without exception, be interpreted and understood based on how a given feature, such as crack speed, temperature, or a material property, affects the stress at which transformation occurs. A simple model was introduced showing that the toughness enhancement could be expressed to leading order as  $G_{ss} \approx G_0(1+c\varepsilon_0 E/\alpha_t^2\sigma_0)$ . For temperatures below the austenite to martensite transition the material is

in the martensite phase and the toughening is insensitive to crack speed and thermal properties because the parameter  $\alpha_t \approx 1$ . The toughening in this phase does depend on the mechanical properties, most notably  $\varepsilon_0 E/\sigma_0$  and  $H_T/\sigma_0$ , with stronger and harder materials having a smaller toughness enhancement. However, at temperatures above the transition temperature when the material is in the austenite phase the transformation stress is very sensitive to temperature, and thus  $\alpha_t$ . Features of the problem that tend to increase the local crack tip temperature, and thus the local transformation stress, also cause decreases in the toughness enhancement due to the reduced transformation zone size near the crack tip and associated reduction in overall dissipated energy.

The primary driver of temperature change during crack growth is the release of latent heat during the stress-induced transformation from austenite to martensite. The thermal properties of the material that tend to keep the temperature change due to this transformation low will also tend to increase the toughening. For example, a large thermal conductivity will reduce the crack tip temperature by allowing the heat to diffuse away into the bulk. This feature sets up a competition between the crack speed and the rate of thermal conduction and is the primary mechanism for the rate dependence of the toughening. Faster cracks will not give enough time for the heat to diffuse away from the tip and thus will show lower toughening. Finally, the heat capacity of the material can also meditate temperature



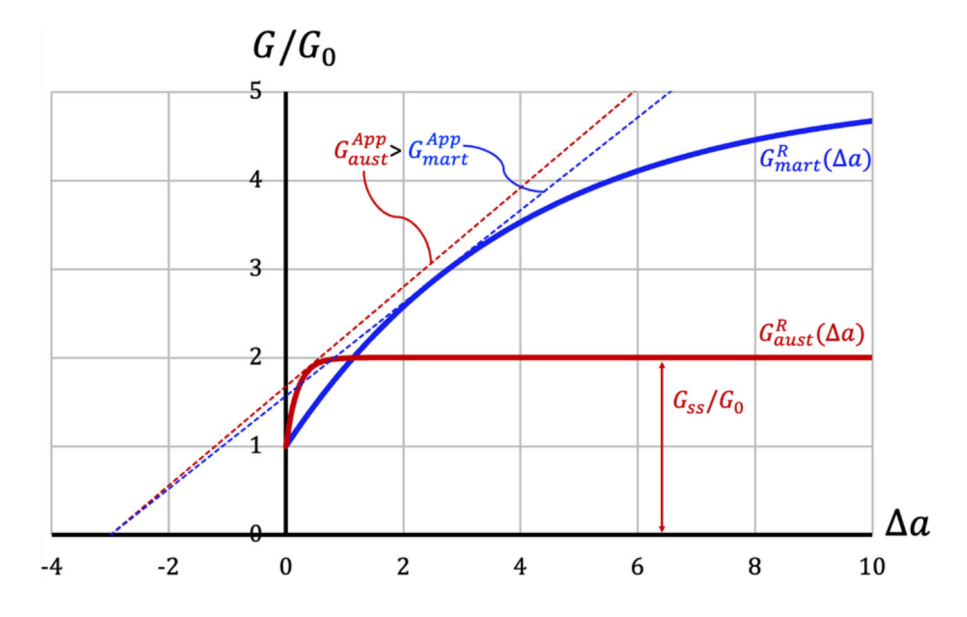
changes near the crack tip since a material with a large heat capacity will have a lower isentropic temperature change during transformation than a low heat capacity material. This explains the final result presented showing that the toughness enhancement increases as the heat capacity of the material increases.

We now return to the experimental measurements that seem to be at odds with the theoretical calculations presented here from Maletta et al. (2016) who found that the measured fracture toughness of the material increased with increasing temperature. However, we also note that Haghgouyan et al. (2019) reported contradictory results finding that the measured toughness of phase-transforming high temperature austenite was lower than that of the low temperature martensite phase. Here we offer some possible explanations. First, as mentioned previously, the intrinsic toughness of the material,  $G_0$  cannot be predicted with the methods used in this work. Instead it is only the ratio of the steady-state toughness to the intrinsic toughness that is calculated, see Fig. 10. Therefore it is possible that a strong increasing dependence of the intrinsic toughness  $G_0$  on increasing temperature could at least offer a partial explanation. Haghgouyan et al. (2019) did find that at very high temperatures where the transformation to martensite no longer occurred the measured fracture toughness did in fact increase. Additionally, the present calculations do not account for any plasticity that may be occurring at the crack tip and any associated interactions between plastic deformation and phase transformation. This may also play a role in the discrepancy

Fig. 10 R-curve behavior showing how a material with large steady-state toughness can have a lower specimen geometry-dependent measured toughness than another material with a lower steady-state toughness

between the present theory and the experimental measurements.

A final possible explanation for the discrepancy between the theoretical toughness enhancement and the experimentally measured toughness has to do with the interaction between the specimen loading/geometry configuration and the details of the shape of the Rcurve. Figure 10 illustrates these issues. Here, the solid red and blue curves are the fracture resistance, i.e. Rcurves, for high temperature austenite and low temperature martensite respectively. Again, we emphasize that these R-curves have not be calculated in this paper, and only the final plateau value of the Rcurve has been computed. Such calculations are left for possible future work. In this schematic the austenite R-curve,  $G_{aust}^{R}(\Delta a)$ , has a steady-state toughness of only twice the intrinsic toughness (where infinitesimal amounts of crack growth first begin), but the amount of crack growth required to develop the transformation zone fully and reach steady state is relatively short. In contrast, the steady-state toughness for the martensite R-curve,  $G_{mart}^{R}(\Delta a)$ , has a large steady state toughness, but a much longer amount of crack growth required to achieve steady-state. In fact, the plateau for the martensite R-curve is not yet achieved for the crack length increments plotted in the figure. For the R-curves shown here the measured fracture toughness will depend on the type of loading and the specimen geometry. Specifically, the conditions for unstable crack growth are that  $G^{App} = G^R$ and  $dG^{App}/d(\Delta a) = dG^R/d(\Delta a)$ , where  $G^{App}$  is





the applied energy release rate which is dependent on crack length a and the applied loading. For example, for a Griffith-type crack,  $G^{App} = \sigma^2 \pi a (1 - v^2)/E$ , where  $\sigma$  is the far field applied tensile stress to an infinite plate with a center-crack of length 2a. Note that for the Griffith crack  $G^{App}$  is linear in  $\Delta a$  and that is the case shown in Fig. 10 by the dashed red and blue lines. What is shown in Fig. 10 is that the crack growth instability conditions are met for the lowsteady-state-toughness austenite material before they are met by the high-steady-state-toughness martensite material. For the case shown in the schematic the measured toughness of the austenite is approximately 7% higher than the measured toughness for the martensite, while the steady-state toughness of the austenite is only 20% of the steady-state toughness of the martensite. While a quantitative analysis of the experiments reported by Maletta et al. (2016) is beyond the scope of this work, their observations that the low temperature martensite sample showed a significant departure from linear behavior prior to peak load while the austenite samples were nearly linear up until fracture does offer qualitative support for this possible explanation. The compliant behavior could be due to either some stable crack growth prior to peak load, as suggested by the R-curve analysis, or to large scale martensite reorientation and detwinning over large regions of the sample. The linear behavior observed in the austenite samples is consistent with very small amounts of stable crack growth prior to the peak load and small contained phase transformation zones around the crack tip.

This discussion suggests that care must be taken when comparing experimental measurements to theoretical calculations such as these, where features of the R-curve beyond simply the steady-state toughness value may be important. This also suggests that experiments with stable crack growth loading/geometries, i.e.  $G^{App}$  decreases with  $\Delta a$ , are of value for a full characterization of the fracture toughness and R-curve behavior of SMA materials. Such experiments would require stiff load frames capable of applying (nearly) displacement-controlled loading as well as precise measurement techniques for determining the location of the crack tip during crack growth. In addition to such experiments, modeling the details of the development of the R-curve behavior in SMAs also remains an open problem.

**Acknowledgements** The authors acknowledge with thanks the financial support received for this work from the National Science Foundation under grant no. CMMI-1762389.

#### References

- Alsawalhi MY, Landis CM (2021) A new phenomenological constitutive model for shape memory alloys. Int J Solids Struct. https://doi.org/10.1016/j.ijsolstr.2021.111264
- Ardakani SH, Ahmadian H, Mohammadi S (2015) Thermomechanically coupled fracture analysis of shape memory alloys using the extended finite element method. Smart Mater Struct 24(4):045031
- Baxevanis T, Landis CM, Lagoudas DC (2014) On the effect of latent heat on the fracture toughness of pseudoelastic shape memory alloys. J Appl Mech 81(10):101006
- Baxevanis T, Landis CM, Lagoudas DC (2014) On the fracture toughness of pseudoelastic shape memory alloys. J Appl Mech 81(4):041005
- Birman V (1998) On mode i fracture of shape memory alloy plates. Smart Mater Struct 7(4):433
- Dean R, Hutchinson J (1980) Quasi-static steady crack growth in small-scale yielding. In: Fracture mechanics: twelfth conference. ASTM International, West Conshohocken
- Haghgouyan B, Hayrettin C, Baxevanis T, Karaman I, Lagoudas DC (2019) Fracture toughness of NiTi-towards establishing standard test methods for phase transforming materials. Acta Mater 162:226–238
- Hutchinson JW (1974) On steady quasi-static crack growth. Tech. Rep. Harvard University, Cambridge
- Irwin G (1960) Plastic zone near a crack and fracture toughness. In: Proceedings of the 7th Sagamore ordnance materials conference (Syracuse University, New York), p IV-63
- Landis CM (2003) On the fracture toughness of ferroelastic materials. J Mech Phys Solids 51(8):1347–1369
- Maletta C, Furgiuele F (2010) Analytical modeling of stressinduced martensitic transformation in the crack tip region of nickel-titanium alloys. Acta Mater 58(1):92–101
- Maletta C, Sgambitterra E, Niccoli F (2016) Temperature dependent fracture properties of shape memory alloys: novel findings and a comprehensive model. Sci Rep 6(1):1–11
- McMeeking R, Evans A (1982) Mechanics of transformationtoughening in brittle materials. J Am Ceram Soc 65(5):242– 246
- Yi S, Gao S (2000) Fracture toughening mechanism of shape memory alloys due to martensite transformation. Int J Solids Struct 37(38):5315–5327
- You Y, Gu X, Zhang Y, Moumni Z, Anlaş G, Zhang W (2019) Effect of thermomechanical coupling on stress-induced martensitic transformation around the crack tip of edge cracked shape memory alloy. Int J Fract 216(1):123–133
- Zaki W, Moumni Z (2007) A three-dimensional model of the thermomechanical behavior of shape memory alloys. J Mech Phys Solids 55(11):2455–2490

**Publisher's Note** Springer Nature remains neutral with regard to jurisdictional claims in published maps and institutional affiliations.

